The Astronomical Journal, 131:939–950, 2006 February

# IN SEARCH OF CIRCUMSTELLAR DISKS AROUND YOUNG MASSIVE STARS

Luis A. Zapata,[1,2] Luis F. Rodríguez,[1] Paul T. P. Ho,[2,3] Henrik Beuther,[2,4] and Qizhou Zhang[2]

*Received 2005 September 4; accepted 2005 October 26*

## ABSTRACT

We present 7 mm, 1.3 cm, and 3.6 cm continuum observations made with the Very Large Array toward a sample of 10 luminous *IRAS* sources that are believed to be regions of massive star formation. We detect compact 7 mm emission in four of these objects: IRAS 18089−1732(1), IRAS 18182−1433, IRAS 18264−1152, and IRAS 18308−0841, and for the first time find that these *IRAS* sources are associated with double or triple radio sources separated by a few arcseconds. We discuss the characteristics of these sources based mostly on their spectral indices and find that their natures are diverse. Some features indicate that the 7 mm emission is dominated by dust from disks or envelopes. Toward other components, the 7 mm emission appears to be dominated by free-free radiation, both from ionized outflows or from optically thick H ii regions. Furthermore, there is evidence of synchrotron contamination in some of these sources. Finally, we find that the sources associated with ionized outflows or thermal jets are correlated with $CH_3OH$ masers. The precise determination of the nature of these objects requires additional multifrequency observations at high angular resolution. The 3.6 cm continuum observations also revealed seven ultracompact (UC) H ii regions in the vicinity of the sources IRAS 18089−1732(1), and two more in the source IRAS 18182−1433. We show that the small photoionized nebulae of these UC H ii regions are produced by early B-type stars.

*Key words:* ISM: individual (IRAS 18089−1732, IRAS 18182−1433, IRAS 18264−1152, IRAS 18308−0841) — radio continuum: ISM — stars: formation — stars: pre–main-sequence

## 1. INTRODUCTION

Massive stars ($M \geq 10\ M_\odot$) are fundamental in determining the physical and chemical evolution of galaxies. They produce a dominant fraction of the heavy elements, generate large amounts of UV radiation during their lives, and inject turbulent energy into the Galactic interstellar medium (ISM). However, the formation of massive stars is a poorly understood phenomenon. Schematically, there are two scenarios that have been proposed to explain the formation of massive stars. The first is the accretion scenario (Garay & Lizano 1999; Norberg & Maeder 2000; McKee & Tan 2002), similar to that operating for low-mass stars, in which a dynamical collapse of molecular clumps results in the formation of disks and molecular outflows, which leads to the formation of a stellar core. In contrast to this, the coalescence scenario (Bonnell et al. 1998; Stahler et al. 2000; Bally & Zinnecker 2005) proposes that massive stars form by the merging of stars of low and intermediate masses. The possible existence of this coalescence scenario receives support from two facts: (1) for a spherically symmetric geometry, the radiation pressure can reverse the infall process once the central star reaches about 10 $M_\odot$ (Wolfire & Cassinelli 1987; see, however, Yorke & Sonnhalter [2002] for models that can produce stars with larger masses) and (2) most massive stars are born in the center of dense clusters of low- and intermediate-mass stars (Bonnell et al. 1998 and references therein). While the accretion scenario implies the existence of well-formed disks and jets, this is not the case for the coalescence scenario, in which disks and jets are expected to be disrupted during the merging.

In recent years there has been a large effort to find observational evidence to discriminate between the two scenarios. Searches have been carried out to find evidence for rotating disks using Very Large Array (VLA) ammonia observations. In two out of 12 objects studied, both B-type protostars, Zhang et al. (1998, 2002) found evidence for signatures of rotating disks. Pestalozzi et al. (2004) have interpreted VLBI observations of methanol masers in NGC 7538 IRS1 in terms of an edge-on Keplerian disk extending to a radius of ∼1000 AU and orbiting a 30 $M_\odot$ protostar. However, the methanol masers often seem to be associated with shocked molecular gas (De Buizer 2003; Kurtz et al. 2004). Gibb et al. (2004) have tried imaging dusty disks using subarcsecond Berkeley-Illinois-Maryland Association millimeter array observations (at 2.7 and 1.4 mm wavelengths) toward eight massive objects. In most of the objects, they found that even at 2.7 mm the dominant emission mechanism is free-free continuum from a thermal jet. Moreover, if other OB-type stars have been formed previously in the region, the object studied may be in the vicinity of bright free-free emission that will make it very difficult to search for the relatively weak millimeter emission from the disk. Finally, the shorter photoevaporation timescale of disks, the large distances (≥1 kpc), and the heavy extinctions ($A_V \geq 100$) have also been inherently difficult problems in the search for disks around high-mass protostars.

At present, there is a list of early B-type protostars that have been associated with possible circumstellar disks, e.g., the BN object (Jiang et al. 2005), Cepheus A HW2 (Patel et al. 200), IRAS 20126+4140 (Cesaroni et al. 1997, 1999; Zhang et al. 1998, 2002), IRAS 18089−1732 (Beuther et al. 2004b; Beuther 2005), IRAS 18182−1433 (H. Beuther et al. 2006; Q. Zhang et al. 2006, both in preparation), G192.16−3.82 (Shepherd et al. 2001); W33A, AFGL 2591 and NGC 7538 IRS9 (Van der Tak & Menten 2005), AFGL 5142 (Zhang et al. 2002), AFGL 490 (Schreyer et al. 2002 and K. Schreyer et al. 2006, in preparation).

We note that sources IRAS 18089−1732 and IRAS 18182−1433 are remarkable examples of massive protostars that are

---

[1] Centro de Radioastronomía y Astrofísica, Dirección General de Asuntos del Personal Académico (DGAPA), of Universidad Nacional Autónoma de México, Apartado Postal 3-72 (Xangari), 58089 Morelia, Michoacán, Mexico; lzapata@astrosmo.unam.mx.

[2] Harvard-Smithsonian Center for Astrophysics, 60 Garden Street, Cambridge, MA 02138.

[3] Academia Sinica Institute of Astronomy and Astrophysics, Taipei, Taiwan.

[4] Max Planck Institute for Astronomy, Königstuhl 17, 69117 Heidelberg, Germany.

TABLE 1

Physical Parameters of the 10 Selected 1.2 mm Continuum Sources

| | Coordinates | | | Physical Parameters | |
|---|---|---|---|---|---|
| Source | $\alpha_{2000}$ | $\delta_{2000}$ | Distance[a] (kpc) | Luminosity ($L_\odot$) | Core Mass[b] ($M_\odot$) |
| IRAS 18089−1732(1)[c] ........ | 18 11 51.3 | −17 31 29 | 3.6 | $3.2 \times 10^4$ | 1200 |
| IRAS 18089−1732(4) ......... | 18 12 30.4 | −17 32 59 | 3.6 | . . . | 200 |
| IRAS 18090−1832 ............. | 18 12 01.9 | −18 31 56 | 6.6 | $1.3 \times 10^4$ | 1000 |
| IRAS 18182−1433 ............. | 18 21 07.9 | −14 31 53 | 4.5 | $2.0 \times 10^4$ | 1500 |
| IRAS 18264−1152 ............. | 18 29 14.3 | −11 50 26 | 3.5 | $1.0 \times 10^4$ | 2200 |
| IRAS 18290−0924 ............. | 18 31 44.8 | −09 22 09 | 5.3 | $2.5 \times 10^4$ | 800 |
| IRAS 18308−0841 ............. | 18 33 31.9 | −08 39 17 | 4.9 | $1.6 \times 10^4$ | 1300 |
| IRAS 18521+0134 .............. | 18 54 40.8 | 01 38 02 | 5.0 | $1.3 \times 10^4$ | 500 |
| IRAS 18553+0414 .............. | 18 57 52.9 | 04 18 06 | 0.6 | $2.5 \times 10^2$ | 15 |
| IRAS 19012+0536 .............. | 19 03 45.1 | 05 40 40 | 4.6 | $1.6 \times 10^4$ | 500 |

Note.—Units of right ascension are hours, minutes, and seconds, and units of declination are degrees, arcminutes, and arcseconds. These parameters were obtained from Sridharan et al. (2002).

[a] This distance listed is the nearest distance, and the luminosity and core mass were calculated with this distance.

[b] The masses listed here are a factor of 2 less than calculated by Beuther et al. (2002a). This difference is because Beuther et al. (2002a) use a sightly different procedure to calculate the total mass of the cores than the one developed by Hildebrand (1983). See the erratum for Beuther et al. (2002a).

[c] This source was previously known as IRAS 18089 − 1732; however, we have added a number (1) at the end of the name to distinguish between this component and component IRAS 18089 − 1732(4).

associated with possible circumstellar disks that are further discussed below.

In this paper we present a centimeter and millimeter wavelength continuum study of 10 *IRAS* sources that are thought to be regions of massive star formation. The purpose of this research is to identify the nature of these massive sources and to select a subset of good candidates for having associated a circumstellar disk.

## 2. THE SAMPLE

The ten IRAS regions observed were selected from the sample of 69 high-mass protostellar objects of Sridharan et al. (2002) using the following criteria: high luminosity ($\sim 2 \times 10^4\ L_\odot$), suggesting the presence of OB-type protostars; compact size in their millimeter emission ($\leq 20'' \times 20''$); proximity to the Sun (a few kpc or less); bright flux density at 1.2 mm ($\geq 200$ mJy); and weak centimeter emission ($\leq 1$ mJy). The criterion of weak centimeter emission was included to search for sources where the continuum emission at 7 mm and shorter wavelengths from possible disks is less likely to be contaminated by free-free emission. In Table 1 we show the main properties of the 10 objects selected.

## 3. OBSERVATIONS

The observations were made with the VLA of NRAO[5] in the continuum mode at 7 mm on 2004 April 1, and at 1.3 cm and 3.6 cm on 2004 May 17. At these epochs, the VLA was in its C configuration. The absolute flux calibrator was 1331+305. In Tables 2, 3, and 4 we present a summary of the observations that are discussed here, including the measured flux density of the phase calibrators.

As mentioned above, during the first epoch we made 7 mm continuum observations toward the 10 selected massive young regions. We detected continuum emission at or above a 3 $\sigma$ level of ~0.5 mJy in four of the regions: IRAS 18089–1732(1), IRAS

TABLE 2

Parameters of the VLA 0.7 cm Continuum Observations

| | Phase Center | | | | | Synthesized Beam | |
|---|---|---|---|---|---|---|---|
| Source | $\alpha_{2000}$ | $\delta_{2000}$ | Phase Calibrator | Bootstrapped Flux Density (Jy) | rms Noise (mJy) | Size (arcsec) | P.A. (deg.) |
| 18089−1732(1).............. | 18 11 51.3 | −17 31 29 | 1820−254 | 0.479 ± 0.008 | 0.18 | $1.63 \times 1.08$ | −29 |
| 18089−1732(4).............. | 18 12 30.4 | −17 32 59 | 1820−254 | 0.479 ± 0.008 | 0.16 | $2.11 \times 1.47$ | −33 |
| 18090−1832 .................. | 18 12 01.9 | −18 31 56 | 1820−254 | 0.479 ± 0.008 | 0.18 | $1.99 \times 1.49$ | −30 |
| 18182−1433 .................. | 18 21 07.9 | −14 31 53 | 1832−105 | 0.656 ± 0.006 | 0.19 | $1.90 \times 1.59$ | −30 |
| 18264−1152................... | 18 29 14.3 | −11 50 26 | 1832−105 | 0.656 ± 0.006 | 0.18 | $1.84 \times 1.62$ | −28 |
| 18290−0924 .................. | 18 31 44.8 | −09 22 09 | 1832−105 | 0.656 ± 0.006 | 0.16 | $1.37 \times 1.14$ | −10 |
| 18308−0841 .................. | 18 33 31.9 | −08 39 17 | 1832−105 | 0.656 ± 0.006 | 0.22 | $1.77 \times 1.64$ | −14 |
| 18521+0134 ................... | 18 54 40.8 | 01 38 02 | 1851+005 | 0.79 ± 0.01 | 0.13 | $1.35 \times 1.18$ | −9 |
| 18553+0414 ................... | 18 57 52.9 | 04 18 06 | 1851+005 | 0.79 ± 0.01 | 0.13 | $1.38 \times 1.20$ | −22 |
| 19012+0536 ................... | 19 03 45.1 | 05 40 40 | 1851+005 | 0.79 ± 0.01 | 0.12 | $1.36 \times 1.19$ | −30 |

Note.—Units of right ascension are hours, minutes, and seconds, and units of declination are degrees, arcminutes, and arcseconds.

---

[5] The National Radio Astronomy Observatory is a facility of the National Science Foundation operated under cooperative agreement by Associated Universities, Inc.

TABLE 3

Parameters of the 1.3 cm VLA Continuum Observations

| | Phase Center | | | | | Synthesized Beam | |
|---|---|---|---|---|---|---|---|
| Source | $\alpha_{2000}$ | $\delta_{2000}$ | Phase Calibrator | Bootstrapped Flux Density (Jy) | rms Noise ($\mu$Jy) | Size (arcsec) | P.A. (deg.) |
| 18089−1732(1) | 18 11 51.3 | −17 31 29 | 1820−254 | 0.626 ± 0.003 | 70 | 1.73 × 0.94 | 15 |
| 18182−1433 | 18 21 07.9 | −14 31 53 | 1832−105 | 0.981 ± 0.006 | 70 | 2.35 × 1.63 | 28 |
| 18264−1152 | 18 29 14.3 | −11 50 26 | 1832−105 | 0.981 ± 0.006 | 60 | 2.38 × 1.63 | 31 |
| 18308−0841 | 18 33 31.9 | −08 39 17 | 1832−105 | 0.981 ± 0.006 | 170 | 2.44 × 1.63 | 36 |

Note.—Units of right ascension are hours, minutes, and seconds, and units of declination are degrees, arcminutes, and arcseconds.

18182−1433, IRAS 18264−1152, and IRAS 18308−0841. During the second epoch we observed at 1.3 and 3.6 cm wavelengths toward these four regions.

The data were edited and calibrated in the standard manner using the software package Astronomical Image Processing System (AIPS) of NRAO. Clean maps were obtained using the task *imagr* of AIPS. For the 7 mm continuum maps we used the ROBUST parameter set to 5, which corresponds to natural weighting, to achieve maximum sensitivity in each continuum image. In the 1.3 and 3.6 cm continuum maps we used the ROBUST parameter set to 0, for optimal compromise between sensitivity and angular resolution. The contour and gray-scale maps at 0.7, 1.3, and 3.6 cm of the four regions are shown in Figures 1, 2, 4, 5, 7, 8, 10, and 11. The resulting rms noises and synthesized beam parameters for the 0.7, 1.3, and 3.6 cm continuum images are also given in Tables 2, 3, and 4. In addition, in all 7 mm maps we have also applied a (*u, v*)-tapering between 100 to 200 k$\lambda$ in order to increase the signal-to-noise ratio of the extended emission ($\geq 1''$) in these regions.

## 4. RESULTS AND DISCUSSION

In what follows, we discuss separately each of the four sources detected at 7 mm. Our discussion of the spectral indices is based on the assumption that the flux densities did not change between the 2004 April 1 and May 17 observations.

### 4.1. *IRAS 18089−1732(1)*

This source was previously known as IRAS 18089−1732; however, we have added a number (1) at the end of the name to distinguish between this component and component IRAS 18089−1732(4) This region contains a strong and extended ($\sim 11''$) 1.2 mm continuum source, $H_2O$ and Class II $CH_3OH$ maser spots, and a compact ($\sim 1''$) 3.6 cm continuum source that is centered at the middle of the extended 1.2 mm continuum source (Beuther et al. 2002a, 2002d). In recent millimeter and submillimeter observations made with the Submillimeter Array (SMA), Beuther et al. (2004b) and Beuther (2005) found a 1.2 mm continuum compact core elongated in the southeast-northwest direction, while in the 860 $\mu$m continuum observations they detected more compact emission, that is coincident with the 3.6 cm source and the $H_2O$ maser (see Beuther et al. 2004b, Fig. 1). Furthermore, Beuther et al. (2004b) and Beuther (2005) found a molecular line forest associated with this source; particularly, the $HCOOCH_3$ (20–19) line appears to show evidence for the signatures of rotation. Finally, IRAM 30 m single-dish SiO $J = 2 \rightarrow 1$ (H. Beuther 2005, private communication) and SMA SiO $J = 5 \rightarrow 4$ (Beuther et al. 2004b) observations show evidence of outflowing molecular gas emanating from this region.

The 7 mm maps (see Figs. 1 and 2) show that this source is actually a double source with components separated by approximately $2''$ (7200 AU, at a distance of 3.6 kpc) in the northeast-southwest direction. We refer to these components as IRAS 18089−1732(1)a and IRAS 18089−1732(1)b.

In Figure 2 we have overlaid the 1.2 and 0.86 mm continuum maps from Beuther et al. (2004b) with our 7 mm continuum maps. Figures 2*A* and 2*B* show that the 1.2 and 0.87 mm continuum cores found by Beuther et al. are associated with the compact 7 mm continuum source IRAS 18089−1732(1)a. We now discuss each subcomponent separately.

#### 4.1.1. *IRAS 18089−1732(1)a*

The radio source IRAS 18089−1732(1)a is resolved in the 7 mm maps. It has deconvolved dimensions of $2\farcs3 \pm 0\farcs4 \times 1\farcs1 \pm 0\farcs4$ and a position angle $= 28° \pm 15°$. In the 1.3 cm continuum maps we detect the counterpart of IRAS 18089−1732(1)a (see Fig. 1*B*). This source is also resolved and has deconvolved dimensions of $1\farcs4 \pm 0\farcs2 \times 0\farcs9 \pm 0\farcs2$ and a P.A. $= 32° \pm 13°$. The position angle of the source is similar at 7 mm and 1.3 cm, as well as to the position angle of the monopolar SiO outflow reported by Beuther et al. (2004a).

The 3.6 cm continuum map also shows a source that is coincident with IRAS 18089−1732(1)a (see Fig. 1*A*); however, with our resolution ($\sim 4''$) we cannot resolve it. From Figure 1 of Beuther et al. (2004a) and our Figures 1 and 2, we associate this 3.6 cm

TABLE 4

Parameters of the VLA 3.6 cm Continuum Observations

| | Phase Center | | | | | Synthesized Beam | |
|---|---|---|---|---|---|---|---|
| Source | $\alpha_{2000}$ | $\delta_{2000}$ | Phase Calibrator | Bootstrapped Flux Density (Jy) | rms Noise ($\mu$Jy) | Size (arcsec) | P.A. (deg.) |
| 18089−1732(1) | 18 11 51.3 | −17 31 29 | 1820−254 | 0.771 ± 0.002 | 40 | 4.70 × 2.75 | 17 |
| 18182−1433 | 18 21 07.9 | −14 31 53 | 1832−105 | 1.415 ± 0.004 | 55 | 4.75 × 2.62 | 24 |
| 18264−1152 | 18 29 14.3 | −11 50 26 | 1832−105 | 1.415 ± 0.004 | 40 | 4.90 × 2.66 | 31 |
| 18308−0841 | 18 33 31.9 | −08 39 17 | 1832−105 | 1.415 ± 0.004 | 160 | 4.40 × 2.68 | 28 |

Note.—Units of right ascension are hours, minutes, and seconds, and units of declination are degrees, arcminutes, and arcseconds.

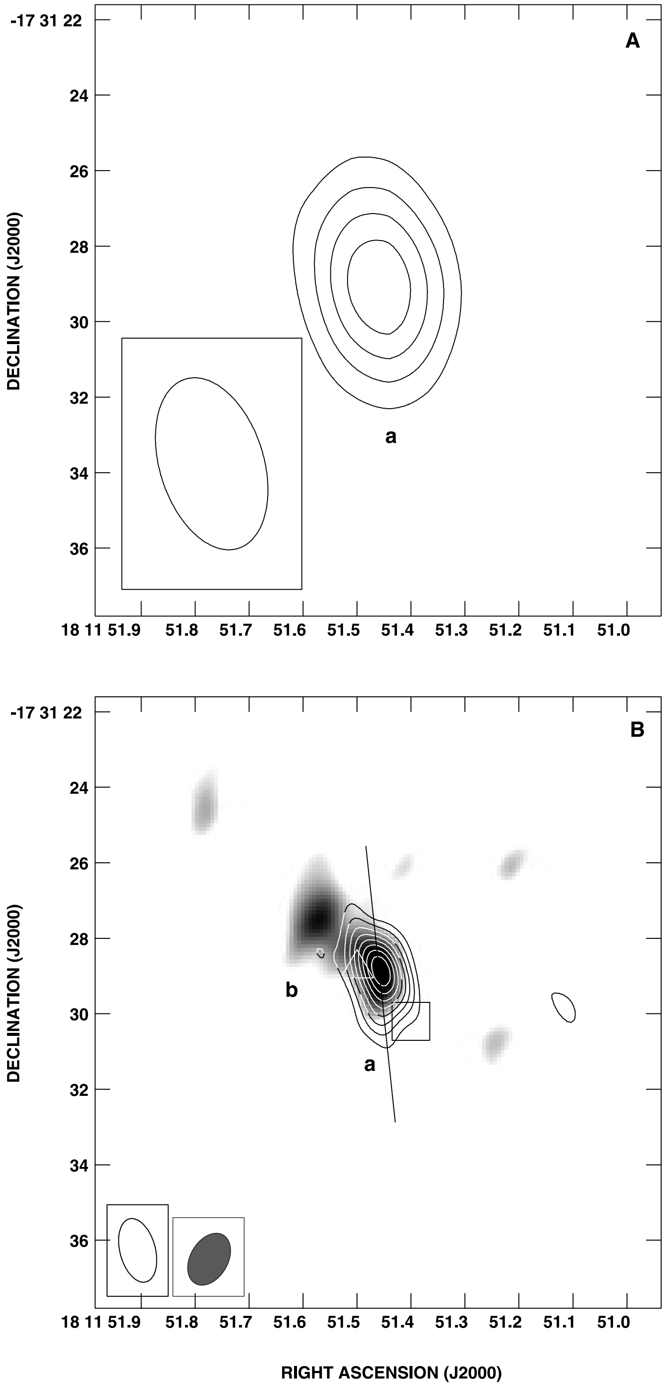

Fig. 1.—VLA continuum images of the source IRAS 18089−1732(1). (*A*) The 3.6 cm continuum emission. The contours are −4, 4, 6, 8, and 10 times 40 $\mu$Jy beam$^{-1}$, the rms noise of the image. (*B*) The 1.3 cm continuum emission (*contours*) and 7 mm continuum emission (*gray scale*). The contours are −4, 4, 6, 8, 10, 12, 14, 16, and 18 times 70 $\mu$Jy beam$^{-1}$, the rms noise of the image. The half-power contour of the synthesized beam is shown in the bottom left corner of each image. The 7 mm continuum map has a (*u*, *v*)-tapering of 200 k$\lambda$. The square and triangle indicate $CH_3OH$ and $H_2O$ maser positions (Walsh et al. 1998; Beuther et al. 2002c), respectively. The line indicates the direction of the SiO molecular outflow found by Beuther et al. (2004b).

continuum source with the source found previously by Beuther et al. (2002b) at the same wavelength. Moreover, the flux densities for both epochs are quite similar: ~1 mJy.

Figure 3*A* shows the spectral energy distribution (SED) for IRAS 18089−1732(1)a from the centimeter to submillimeter wavelengths. It shows a "combined," two-regime spectrum in

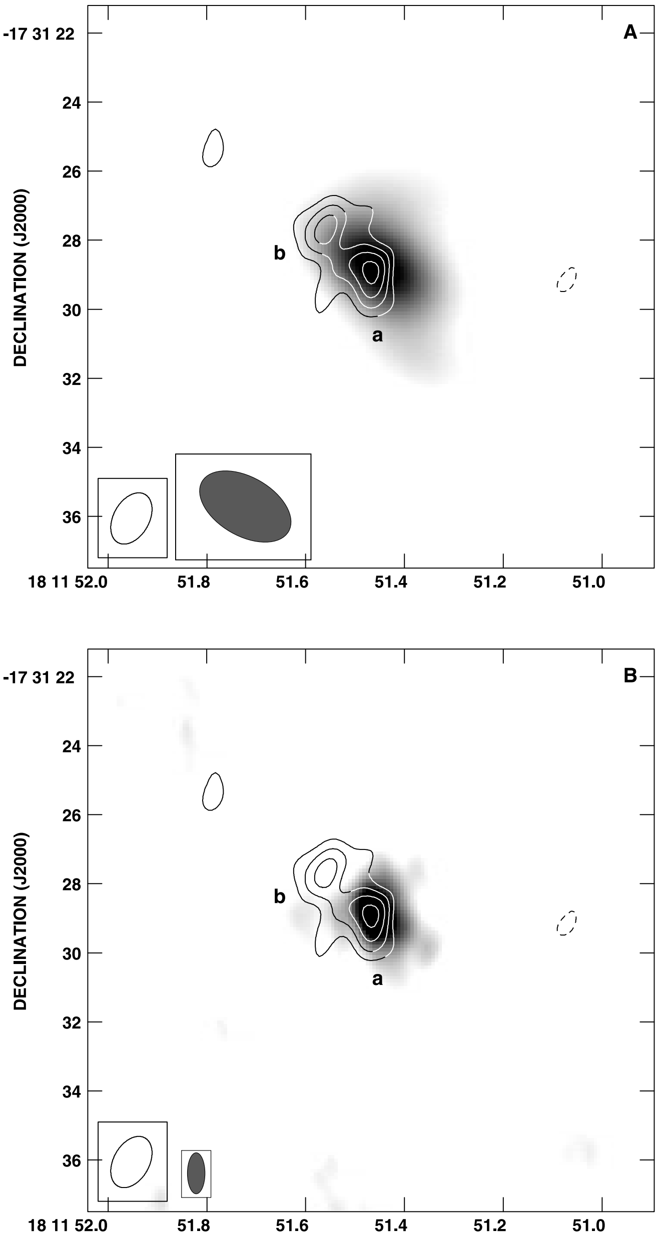

Fig. 2.—VLA and SMA continuum images of the source IRAS 18089−1732(1). The contours show the 7 mm continuum emission, and the gray scale shows the SMA continuum emission at (*A*) 1.2 mm and (*B*) 860 $\mu$m (Beuther et al. 2004b; Beuther 2005). The half-power contour of the synthesized beam is shown in the bottom left corner of each image. The contours are −4, 4, 5, 6, 7, and 8 times 0.19 mJy beam$^{-1}$, the rms noise of the image. The 7 mm continuum map has a (*u, v*)-tapering of 150 k$\lambda$.

which the centimeter emission is dominated by a flat or slowly rising spectrum ($\alpha = 0.58 \pm 0.05$), which can be interpreted as moderately optically thick free-free emission, while the millimeter and submillimeter emission is dominated by a component that rises rapidly with frequency. This component is likely to be associated with dust emission from a core or disk.

Since the orientation of the position angle of IRAS 18089−1732(1)a is in the south-north direction (in the 1.3 cm and 7 mm observations), and its SED at centimeter wavelengths suggests that this source may be associated with a thermal jet or stellar wind, we interpret this source as a thermal jet that is possibly driving the north-south SiO molecular outflow found by Beuther et al. (2004b). Moreover, as we see in our sample, these free-free

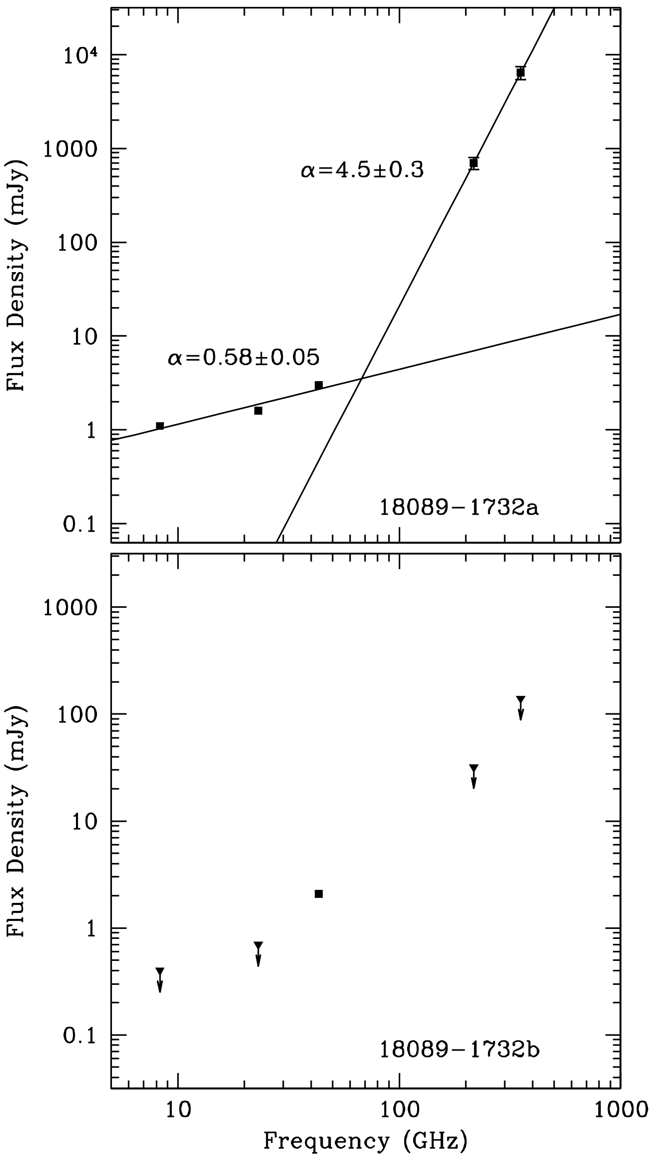

FIG. 3.—SED for each detected radio continuum source in IRAS 18089−1732(1) combining the 0.7, 1.3, and 3.6 cm VLA continuum data and the SMA continuum 1.2 and 0.7 mm data from Beuther et al. (2004a) and Beuther (2005). The squares are detections; the respective error bars were smaller than the squares and are not presented. The triangles with arrows are upper limits (4 $\sigma$). The line is a least-squares power-law fit (of the form $S_\nu \propto \nu^\alpha$) to each spectrum. In the top panel, the 1.2 mm measurement is the peak emission of this source.

emission sources of relatively flat spectrum appear to be systematically associated with $CH_3OH$ maser spots (see Fig. 1*B* and the discussion below).

### 4.1.2. *IRAS 18089−1732(1)b*

This source is reported here for the first time. IRAS 18089−1732(1)b is resolved in the 7 mm maps. It has deconvolved dimensions of $2\farcs7 \pm 0\farcs2 \times 1\farcs6 \pm 0\farcs2$ and a P.A. $= 35° \pm 46°$.

IRAS 18089−1732(1)b is only detected at 7 mm. Figure 3*B* shows its SED from the centimeter to submillimeter wavelengths, mostly as upper limits. From our figures and the SED, this source could be interpreted as associated with dust emission. However, the spectrum of this source seems to flatten between 1.2 mm and 850 $\mu$m (see Fig. 3 and Beuther et al. 2004b). Therefore, we speculate that IRAS 18089−1732(1)b could also be an optically thick H II region that has its turnover frequency at about 100 GHz.

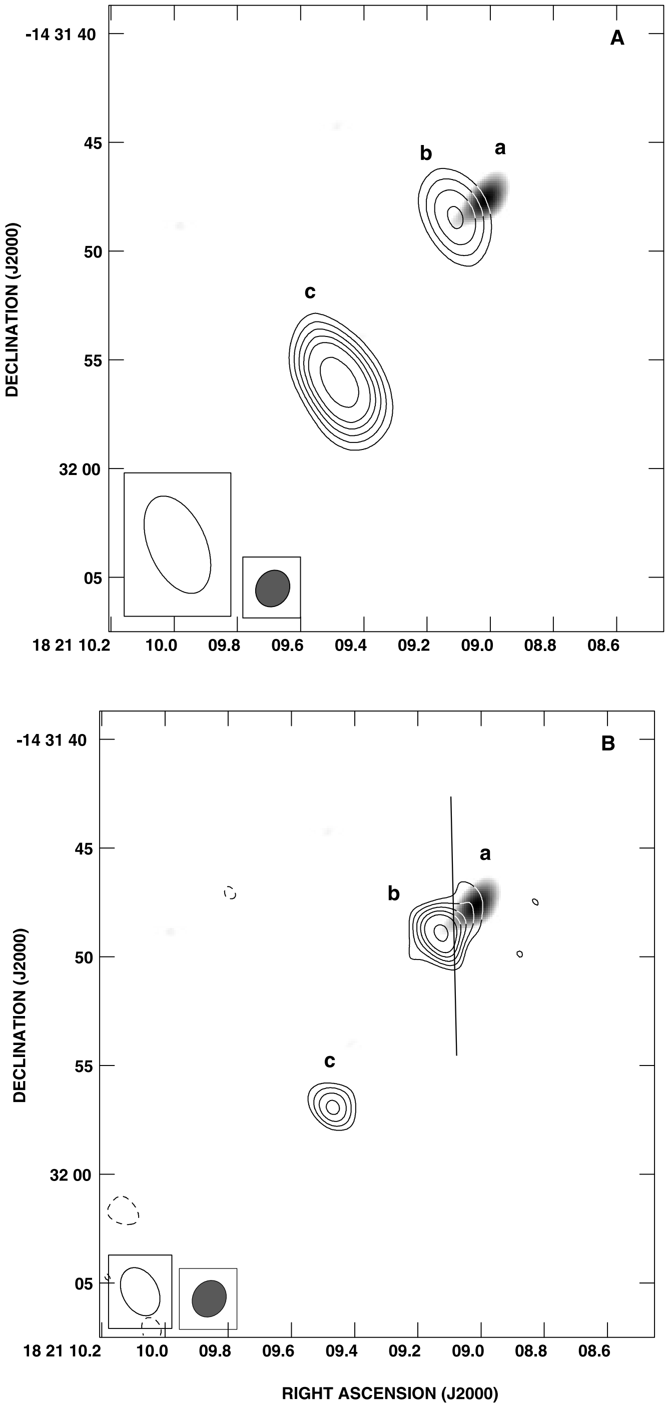

FIG. 4.—VLA continuum images of the source IRAS 18182−1433. (*A*) The contours show the 3.6 cm continuum emission, and the gray scale shows the emission at 7 mm. The contours are −4, 4, 5, 6, 7, 8, and 10 times 55 $\mu$Jy beam$^{-1}$, the rms noise of the image. (*B*) The contours show the 1.3 cm continuum emission, and the gray scale shows the emission at 7 mm. The contours are −4, 4, 5, 6, 7, 8, and 10 times 70 $\mu$Jy beam$^{-1}$, the rms noise of the image. The half-power contour of the synthesized beam is shown in the bottom left corner of each image. The 7 mm continuum maps have a ($u$, $v$)-tapering of 100 k$\lambda$. The line indicates the north-south CO (2−1) molecular outflow found by Beuther et al. (2002b).

### 4.2. *IRAS 18182−1433*

This region contains a strong and extended ($\sim$13″) 1.2 mm continuum source and $H_2O$ and Class II $CH_3OH$ maser spots (Beuther et al. 2002a, 2002d). In recent SMA millimeter continuum and line observations (H. Beuther et al. 2006, in preparation), a compact core ($\sim$4″) has been detected that is also associated

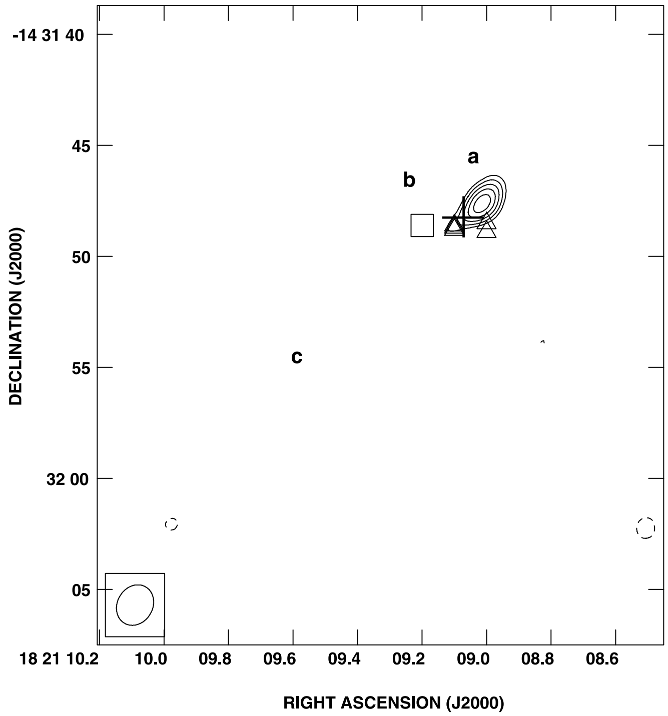

FIG. 5.—VLA continuum image at 7 mm of the source IRAS 18182−1433. The half-power contour of the synthesized beam is shown in the bottom left corner of the image. The contours are −4, 4, 5, 6, 7, and 8 times 0.22 mJy beam$^{-1}$, the rms noise of the image. The square and triangles indicate $CH_3OH$ and $H_2O$ maser positions (Walsh et al. 1998; Beuther et al. 2002d), respectively. This 7 mm continuum map has a ($u$, $v$)-tapering of 100 k$\lambda$. The cross indicates the 1.2 mm continuum emission peak found by H. Beuther et al. (2006, in preparation).

with a molecular line forest. This millimeter continuum core is associated with the $H_2O$ masers. Beuther et al. (2002b) also found an extended (∼1′) CO (2–1) molecular outflow emanating from this region.

The 3.6, 1.3, and 0.7 cm maps (see Figs. 4 and 5) show that IRAS 18182−1433 is a triple source with components separated by 2″–10″. We refer to these components as IRAS 18182−1433a, IRAS 18182−1433b, and IRAS 18182−1433c.

### 4.2.1. *IRAS 18182−1433a*

IRAS 18182−1433a is detected in our 7 mm continuum map but not in our 3.6 cm and 1.3 cm maps above the 4 $\sigma$ level of 55 and 70 $\mu$Jy, respectively. This source is not resolved in the 7 mm continuum map. However, based on our synthesized beam, we set an upper limit of $\leq 2''$ for its angular size.

In Figure 5 we can see that this source is associated with the water masers and the 1.2 mm continuum core found by Beuther et al. (2002a, 2002d). However, there is a shift of about 0″.3 between the two peaks at 7 and 1.2 mm. One possibility is that this shift could be due to the fact that dust emission contribution at 1.2 mm comes from both sources, IRAS 18182−1433a and IRAS 18182−1433b, while the source IRAS 18182−1433b was not detected in our 7 mm continuum map.

Figure 6 (*top*) shows the SED for IRAS 18182−1433a from the centimeter to submillimeter wavelengths. It shows a spectrum associated with a strong dust emission, possibly from the core and disk.

### 4.2.2. *IRAS 18182−1433b*

IRAS 18182−1433b is resolved in our 1.3 cm continuum maps. It has deconvolved dimensions of 1″.7 ± 0″.4 × 1″.4 ± 0″.6 and a P.A. = 87° ± 40°.

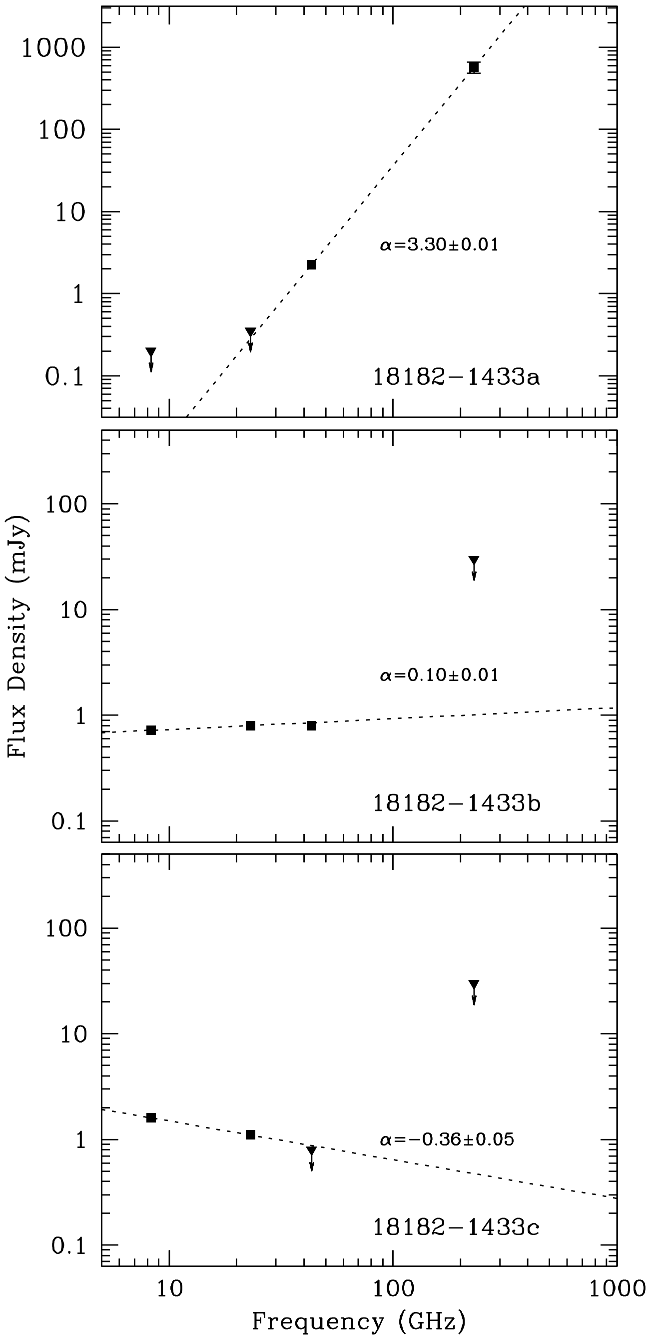

FIG. 6.—SED for each detected radio continuum source in IRAS 18182−1433 combining the 0.7, 1.3, and 3.6 cm VLA continuum data. The squares are detections; the respective error bars were smaller than the squares and are not presented. The triangles with arrows are upper limits (4 $\sigma$). The line is a least-squares power-law fit (of the form $S_\nu \propto \nu^\alpha$) to each spectrum.

IRAS 18182−1433b is not detected in our 7 mm map above a 4 $\sigma$ level of 0.22 mJy. The $CH_3OH$ Class II maser spot found by Beuther et al. (2002d) is associated with this source. Figure 6 (*middle*) shows its SED from the centimeter to submillimeter wavelengths. It shows a slowly rising ($\alpha = 0.10 \pm 0.01$) spectrum. We propose that is produced by free-free emission from a thermal jet or stellar wind. However, this flat spectral index is also consistent with an optically thin H II region.

### 4.2.3. *IRAS 18182−1433c*

This source is not resolved in our 1.3 cm maps. Again, based on our synthesized beam, we set an upper limit of $\leq 2''$ for its

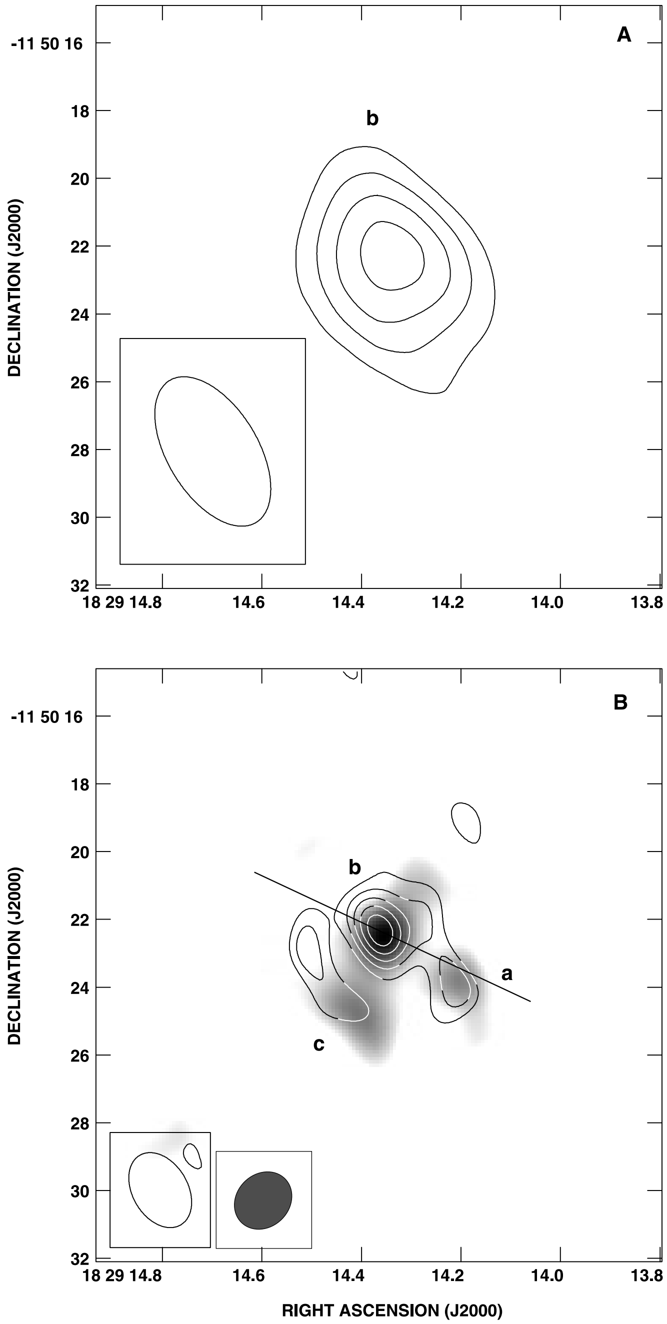

FIG. 7.—VLA continuum images of the source IRAS 18264−1152. (*A*) The 3.6 cm continuum emission. The contours are −4, 4, 6, 8, and 10 times 40 $\mu$Jy beam$^{-1}$, the rms noise of the image. (*B*) The contours show the 1.3 cm continuum emission, and the gray scale shows the emission at 7 mm. The contours are −4, 4, 5, 6, 7, and 8 times 60 $\mu$Jy beam$^{-1}$, the rms noise of the image. The half-power contour of the synthesized beam is shown in the bottom left corner of each image. The 7 mm continuum map has a (*u, v*)-tapering of 100 k$\lambda$. The line indicates the east-west CO (2−1) molecular outflow found by Beuther et al. (2002b).

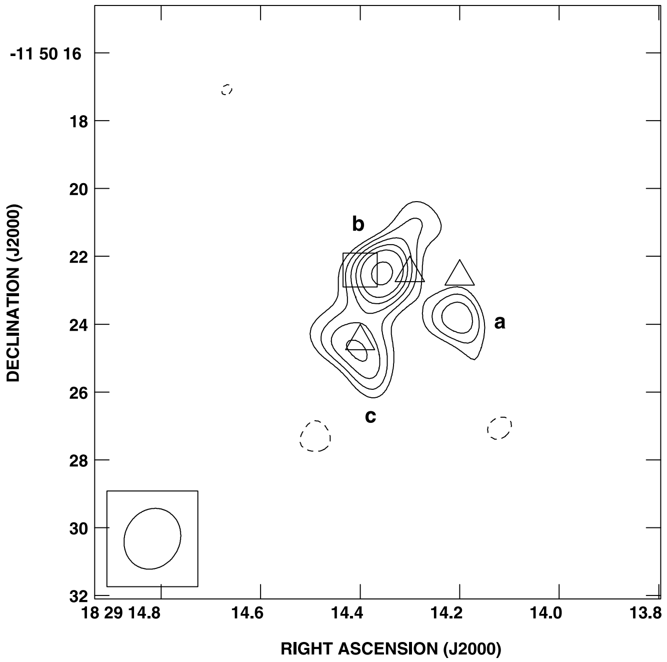

FIG. 8.—VLA continuum image at 7 mm of the source IRAS 18264−1152. The half-power contour of the synthesized beam is shown in the bottom left corner of the image. The contours are −4, 4, 5, 6, 7, 8, and 10 times 0.18 mJy beam$^{-1}$, the rms noise of the image. The square and triangles indicate $CH_3OH$ and $H_2O$ maser positions (Beuther et al. 2002d), respectively. This 7 mm continuum map has a (*u, v*)-tapering of 100 k$\lambda$. It is interesting to note that every 7 mm radio continuum source has an associated $H_2O$ maser spot.

angular size. IRAS 18182−1433c is not detected in our 7 mm map above a 4 $\sigma$ level of 0.22 mJy.

Figure 6 (*bottom*) shows its SED from the centimeter to submillimeter wavelengths. It shows a slightly negative spectrum ($\alpha = -0.36 \pm 0.05$), which is suggestive of nonthermal radiation. Similar negative spectral indices found in sources associated with massive and low-mass star formation are believed to be due to synchrotron contamination from strong shocks (Serpens: Rodríguez et al. 1989; HH 80-81: Martí et al. 1993; Cep A: Garay et al. 1996; W3(OH): Wilner et al. 1999; IRAS 16547−4247: Rodríguez et al. 2005; G192.16−3.82: Shepherd & Kurtz 1999). A detailed discussion on the presence of thermal and nonthermal components in this type of object is given in Garay et al. (1996).

### 4.3. *IRAS 18264−1152*

This region contains a strong and extended (∼15″) 1.2 mm continuum source and $H_2O$ and Class II $CH_3OH$ maser spots (Beuther et al. 2002a, 2002d). IRAS 18264−1152 shows evidence of outflowing activity. Beuther et al. (2002b) found an extended (∼1′) CO (2−1) molecular outflow emanating from here.

The 7 mm and 1.3 cm maps (see Figs. 7 and 8) show that this source is a triple source, with components separated by approximately 2″. We refer to these components as IRAS 18264−1152a, IRAS 18264−1152b, and IRAS 18264−1152c. We propose that they are possibly tracing the components of a triple stellar system.

#### 4.3.1. *IRAS 18264−1152a*

Figure 9 shows the SED of this source from the centimeter to millimeter wavelengths. The power-law index of 2.1 ± 0.05 suggests an optically thick H II region or dust emission from the core and disk.

#### 4.3.2. *IRAS 18264−1152b*

This source is resolved in our 7 mm continuum maps. It has deconvolved dimensions of $3''.8 \pm 0''.5 \times 1''.4 \pm 0''.4$ and a P.A. = $143° \pm 7°$.

Figure 9 shows its SED from the centimeter to millimeter wavelengths. The slightly rising spectrum (spectral index of 0.27 ± 0.06) between 3.6 and 1.3 cm suggests a thermal jet or a partially optically thick H II region. The flux density at 7 mm is much larger than the value extrapolated from the 3.6 and 1.3 cm observations and suggests that dust emission may be dominant at 7 mm.

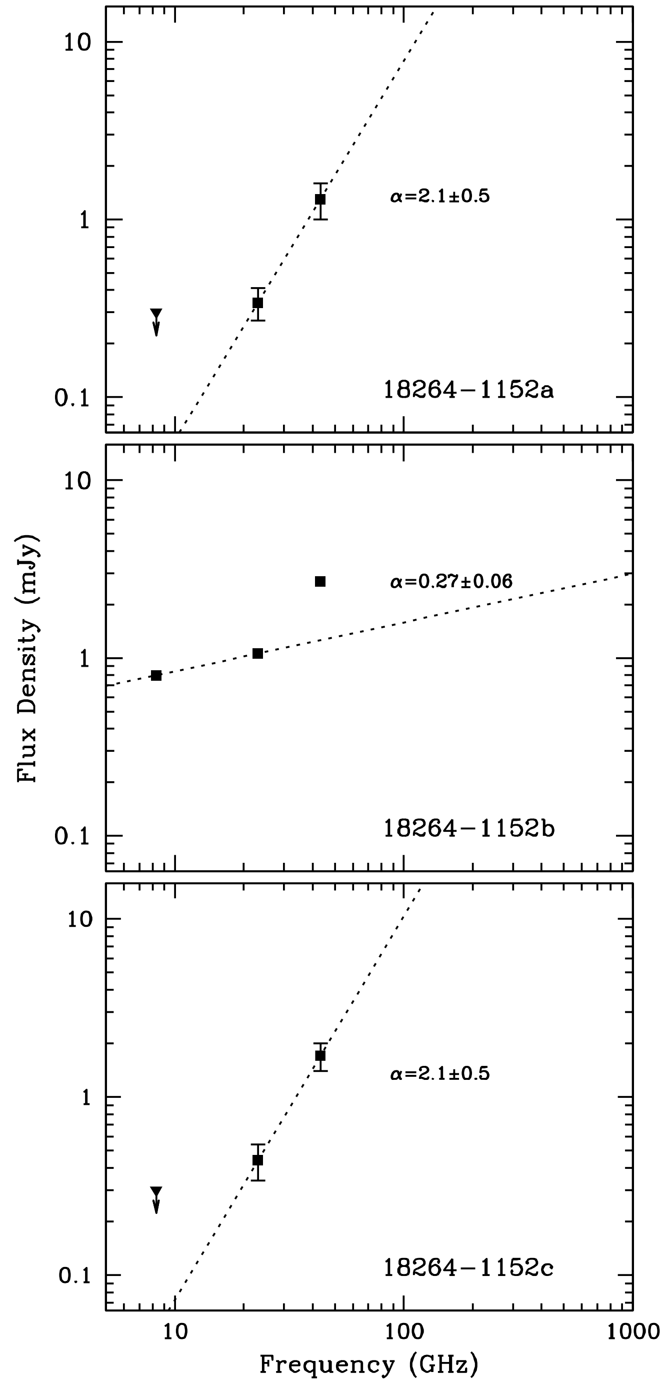

FIG. 9.—SED for each detected radio continuum source in IRAS 18264−1152 combining the 0.7, 1.3, and 3.6 cm VLA continuum data. The squares are detections; in a few cases the respective error bars were smaller than the squares and are not presented. The triangles with arrows are upper limits (4 $\sigma$). The line is a least-squares power-law fit (of the form $S_\nu \propto \nu^\alpha$) to each spectrum.

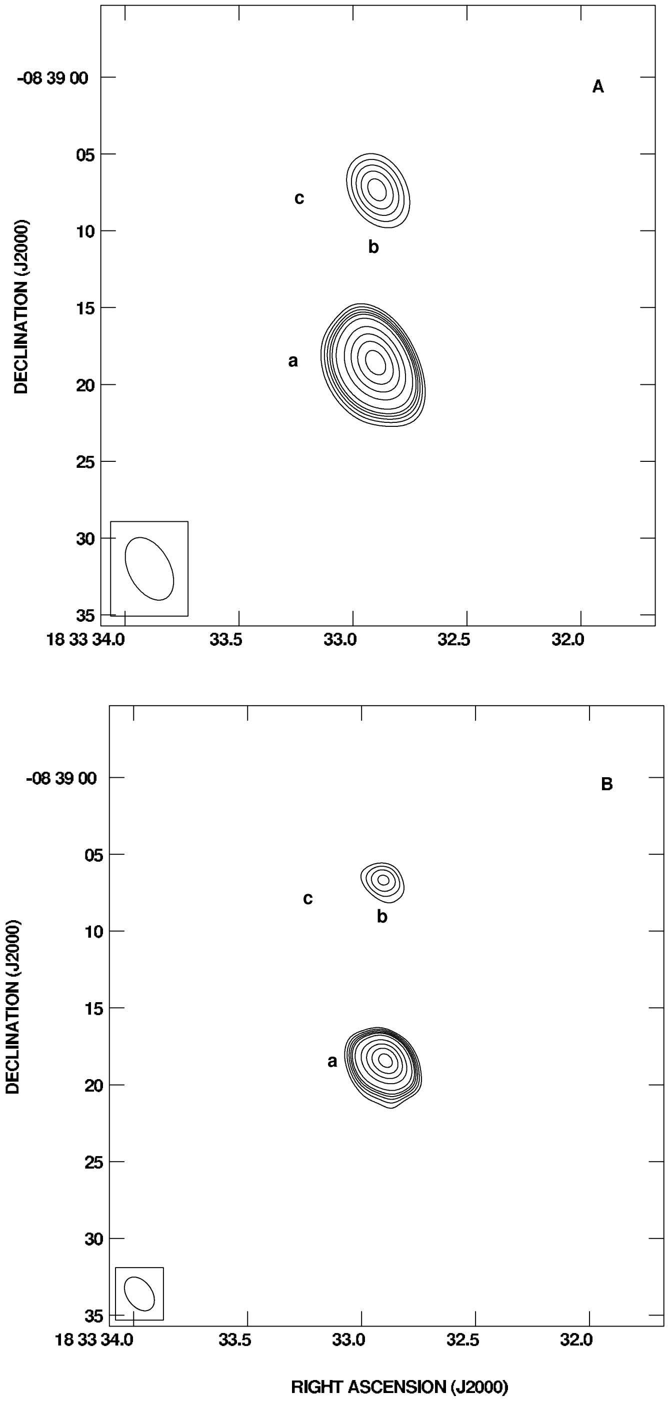

FIG. 10.—VLA continuum images at (*A*) 3.6 and (*B*) 1.3 cm of the source IRAS 18308−0841. The half-power contour of the synthesized beam is shown in the bottom left corner of each image. (*A*) The contours are −4, 4, 6, 8, 10, 12, 14, 16, 18, 20, and 30 times 0.16 mJy beam$^{-1}$, the rms noise of the image. (*B*) The contours are −4, 4, 6, 8, 10, 12, 14, 16, 18, 20, and 30 times 0.17 mJy beam$^{-1}$, the rms noise of the image.

### 4.3.3. *IRAS 18264−1152c*

This source is resolved in our 7 mm continuum maps. It has deconvolved dimensions of $2\farcs4 \pm 0\farcs5 \times 0\farcs9 \pm 0\farcs7$ and a P.A.= $45° \pm 13°$.

Figure 9 shows its SED from the centimeter to millimeter wavelengths. At 3.6 cm, we have only an upper limit. The power-law index of 2.1 ± 0.05 between 1.3 cm and 7 mm suggests an optically thick H II region or dust emission from a core and disk.

### 4.4. *IRAS 18308−0841*

This region contains a strong and extended (~17″) 1.2 mm continuum source and one $H_2O$ maser spot (Beuther et al. 2002a, 2002d). Beuther et al. (2002b) found strong $^{12}$CO (2–1) molecular emission. However, the presence of bipolar outflow structure was not clearly established.

The 7 mm and 1.3 cm maps (see Figs. 10 and 11) show that this source is a triple source with components separated by

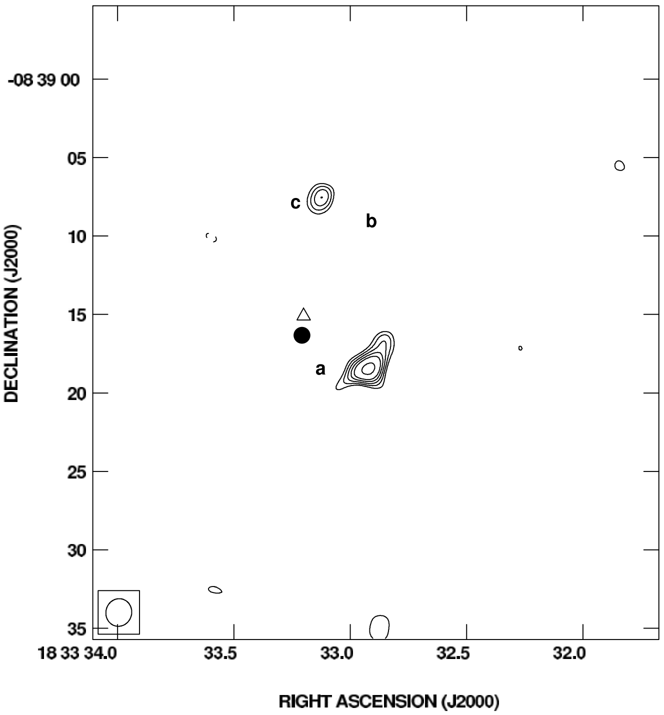

FIG. 11.—VLA continuum image at 7 mm of the source IRAS 18308−0841. The half-power contour of the synthesized beam is shown in the bottom left corner of the image. The contours are −4, 4, 5, 6, 7, 8, and 10 times 0.20 mJy beam$^{-1}$, the rms noise of the image. The triangle indicates the $H_2O$ maser position (Beuther et al. 2002d). This continuum map has a $(u, v)$-tapering of 200 k$\lambda$. The dot indicates the MAMBO 1.2 mm continuum emission peak found by Beuther et al. (2002a)

$3''$–$10''$. We refer to these components as IRAS 18308−0841a, IRAS 18308−0841b, and IRAS 18308−0841c.

### 4.4.1. *IRAS 18308−0841a*

This source is resolved in our 7 mm continuum maps. It has deconvolved dimensions of $2''.16 \pm 0''.04 \times 2''.0 \pm 0''.05$ and a P.A. = 92° ± 14°. This source is also resolved in our 1.3 cm continuum maps. It has deconvolved dimensions of $1''.3 \pm 0''.9 \times 0''.7 \pm 0''.2$ and a P.A. = 100° ± 8°. Finally, the source is also resolved in our 3.6 cm continuum maps. It has deconvolved dimensions of $2''.4 \pm 0''.1 \times 2''.20 \pm 0''.05$ and a P.A. = 60° ± 16°. We find that while the 7 mm and 1.3 cm deconvolved dimensions are consistent, the deconvolved dimensions at 3.6 cm appear to be significantly larger. This may be due to the presence of extended emission that is resolved out or too faint to be detected at 7 mm and 1.3 cm.

Figure 12 shows its SED from the centimeter to millimeter wavelengths. The negative spectral index of −0.42 ± 0.07 could suggest the presence of synchrotron emission. However, this spectral index could also be due to missing flux density in the higher angular resolution and higher frequency observations. Matching-beam observations of the source at several frequencies are needed to discuss the spectral indices in a very reliable way.

### 4.4.2. *IRAS 18308−0841b*

This source is resolved in our 3.6 cm continuum maps. It has deconvolved dimensions of $3''.1 \pm 0''.3 \times 2''.5 \pm 0''.2$ and a P.A. = 75° ± 12°.

Figure 12 shows its SED from the centimeter to millimeter wavelengths. Again, the negative spectral (−0.26 ± 0.01) index could suggest the presence of synchrotron emission. However, this spectral index could also be due to missing flux density in the higher angular resolution and higher frequency observations. Matching-beam observations of the source at several frequencies are also needed to discuss the spectral indices in a very reliable way.

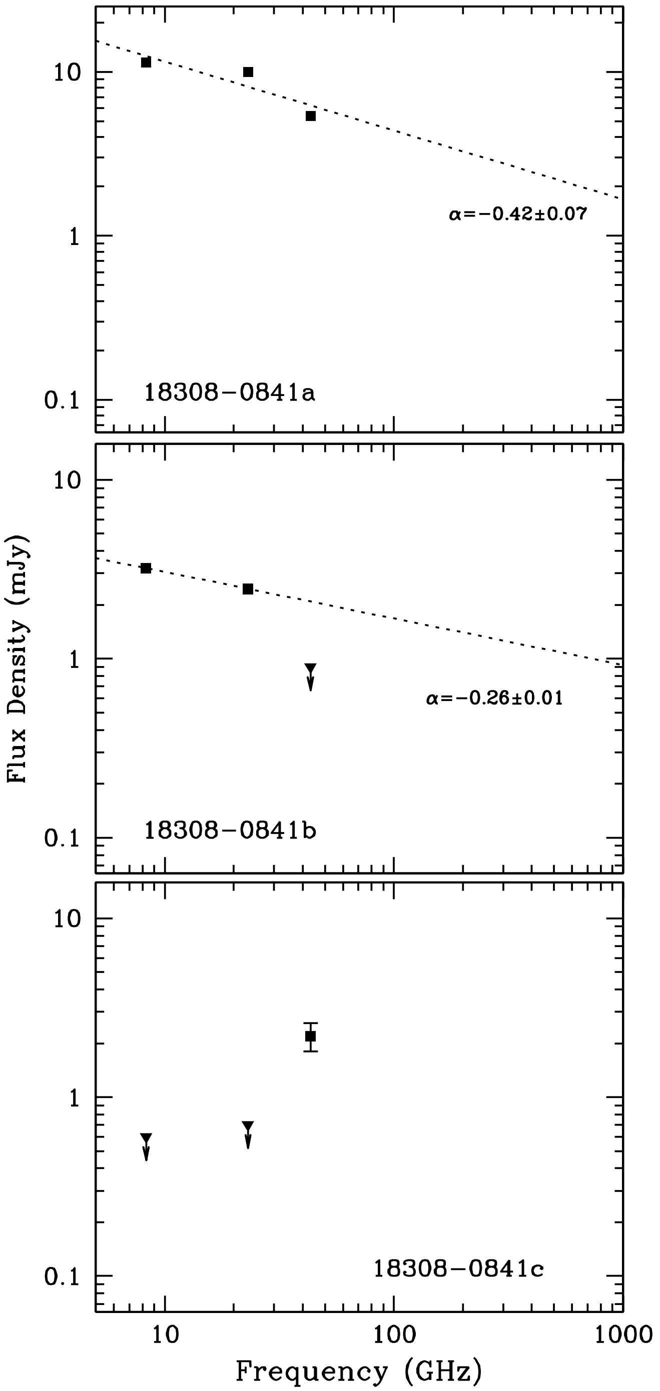

FIG. 12.—SED for each detected radio continuum source in IRAS 18308−0841 combining the 0.7, 1.3, and 3.6 cm VLA continuum data. The squares are detections; in most of the cases the respective error bars were smaller than the squares and are not presented. The triangles with arrows are upper limits (4 $\sigma$). The line is a least-squares power-law fit (of the form $S_\nu \propto \nu^\alpha$) to each spectrum.

### 4.4.3. *IRAS 18308−0841c*

Figure 12 shows its spectral energy distribution from the centimeter to millimeter wavelengths. It was detected only at 7 mm, suggesting that dust is dominant at this wavelength.

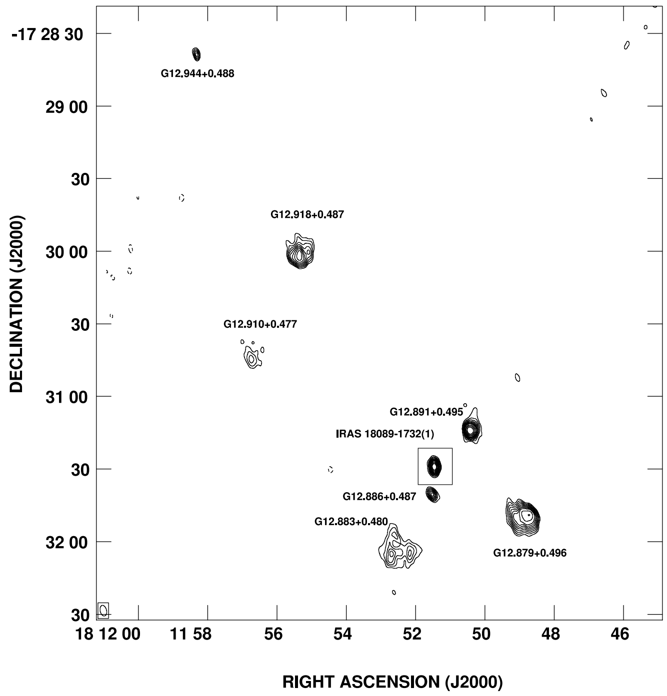

Fig. 13.—VLA continuum image at 3.6 cm toward the source IRAS 18089−1732(1). This map was made with ROBUST = 5 (equivalent to natural weighting). The half-power contour of the synthesized beam is shown in the bottom left corner of the image. The contours are −3, 3, 4, 5, 6, 7, 8, 9, 10, 12, 14, 16, 30, and 60 times 40 $\mu$Jy beam$^{-1}$, the rms noise of the image. The sources G12.879+0.496, G12.891+0.495, G12.886+0.487, G12.918+0.487, G12.918+0.487, G12.910+0.477, and G12.944+0.488 are first reported here. This map was not corrected by primary beam response. The box indicates the approximate size of Fig. 1*A*.

### 4.5. *Clusters of Ultracompact* H II *Regions in the Vicinity of the Sources IRAS 18089−1732(1) and IRAS 18182−1433*

We report for the first time the detection of seven ultracompact (UC) H II regions in the vicinity of the source IRAS 18089−1732(1) and two more UC H II regions in the source IRAS 18182−1433 at 3.6 cm (see Figs. 13 and 14). Their physical parameters are shown in Table 5. Most of them show a cometary or unresolved spherical morphology. Following Van der Tak & Menten (2005), and assuming that the free-free emission is optically thin, that the ionized gas has a temperature of $10^4$ K, and that these sources have distances of 3.6 and 4.5 kpc, we find that the flux of Lyman continuum photons for each UC H II region can be provided by an early B-type star (see Panagia 1973).

We searched for more UC H II regions in the vicinity of the other two *IRAS* sources that were observed at 3.6 cm; however, we did not detect other cases at a 4 $\sigma$ level of their respective rms noises. Therefore, in comparison with these regions, IRAS 18089−1732(1) and IRAS 18182−1433 can be considered rich regions of high-mass star formation.

### 4.6. *General Discussion of the Sources*

With the present angular resolution and sensitivities of our images, it is interesting to note that the four sources detected at 7 mm (IRAS 18089−1732, IRAS 18182−1433, IRAS 18264−1152, and IRAS 18308−0841) are double or triple, with no case of a single source. In the four regions with detected 7 mm emission, we find a total of 11 subcomponents. The spectral index of these subcomponents varies, suggesting different interpretations for the nature of the sources. In Table 6 we give a tentative interpretation for the nature of the sources, based on our discussion.

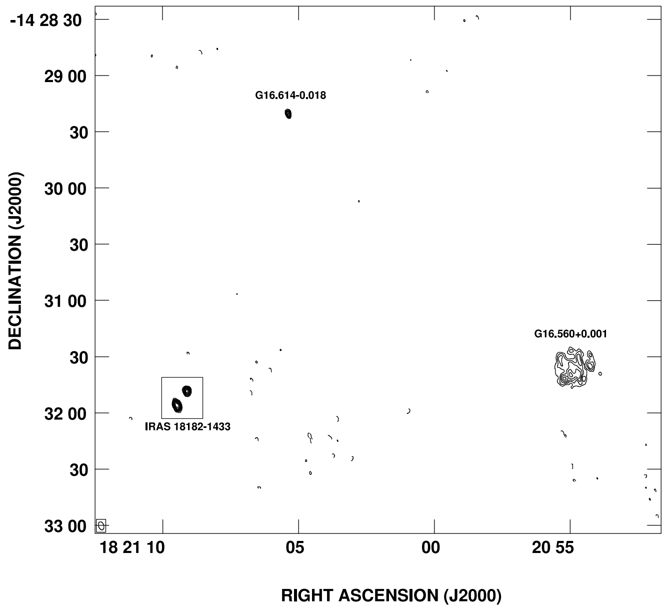

Fig. 14.—VLA continuum image at 3.6 cm toward the source IRAS 18182−1433. This map was made with ROBUST = 5 (equivalent to natural weighting). The half-power contour of the synthesized beam is shown in the bottom left corner of the image. The contours are −3, 3, 4, 5, 6, 7, 8, 9, 10, 12, 14, 16, 30, and 60 times 3.5 $\mu$Jy beam$^{-1}$, the rms noise of the image. The sources G16.560+0.001 and G16.614−0.018 are first reported here. This map was not corrected by primary beam response. The box indicates the approximate size of Fig. 4*A*.

We note that the sources IRAS 18089−1732(1)a, IRAS 18182−1433b, and IRAS 18264−1152b exhibit slightly rising spectral indices which are frequently associated with winds or thermal jets and show a correlation with methanol maser spots. Furthermore, those maser spots are found in the same orientation of the molecular outflows (see Figs. 1*B*, 5, and 8). The methanol masers have already been suggested to be associated with shocked molecular gas in the outflows produced by the star (De Buizer 2003; Kurtz 2004); our data show this correlation and support the notion that the methanol masers are associated with ionized or shocked gas rather than disks (or dust emission).

It is puzzling that we only detected four of the 10 sources observed, since they all (with the exception of IRAS 18553+0414 and IRAS 18089−1732[4]) seem to have similar luminosities and distances. However, these four detected continuum sources (IRAS 18089−1732, IRAS 18182−1433, IRAS 18264−1152, and IRAS 18308−0841) are embedded in the most massive cores of our initial subset (see Table 1).

Of the 11 subcomponents detected, four [IRAS 18089−1732(1)b, IRAS 18182−1433a, IRAS 18264−1152b, and IRAS 18308−0841c] have 7 mm emission that could be coming from the dust.

## 5. CONCLUSIONS

Our main conclusions are summarized below.

1. We mapped 10 regions of massive star formation at 7 mm with the VLA, detecting compact emission in four of them. These four sources were further observed with the VLA at 1.3 and 3.6 cm.

2. Multiplicity is a common factor in the emission detected: three of the four sources detected are resolved into three subcomponents, while the fourth source is a double source.

3. Four of the sources detected show 7 mm emission above the value extrapolated from the observations at longer wavelengths

TABLE 5

Physical Parameters of the H ii Regions Detected with the VLA at 3.6 cm

| | | | Physical Parameters | | | |
|---|---|---|---|---|---|---|
| Source | $\alpha_{2000}$ | $\delta_{2000}$ | Deconvolved Size | P.A. (deg.) | Flux Density (mJy) | $\log(N_{\mathrm{L}})$[a] ($\mathrm{s}^{-1}$) |
| G12.879+0.496 | 18 11 48.834 | −17 31 49.07 | $7.4 \pm 0.5 \times 5.2 \pm 0.5$ | 75° ± 10° | 6.0 ± 0.1 | 45.7 |
| G12.891+0.495 | 18 11 50.422 | −17 31 14.12 | $3.0 \pm 0.3 \times 2.3 \pm 0.6$ | 115° ± 68° | 3.0 ± 0.1 | 45.5 |
| G12.886+0.487 | 18 11 51.510 | −17 31 40.57 | $6.4 \pm 1.4 \times 3.7 \pm 1.5$ | 58° ± 25° | 1.0 ± 0.1 | 45.0 |
| G12.883+0.480 | 18 11 52.680 | −17 32 04.92 | $9.0 \pm 0.8 \times 8.0 \pm 0.7$ | 16° ± 50° | 6.0 ± 0.1 | 45.7 |
| G12.918+0.487 | 18 11 55.360 | −17 30 01.92 | $6.0 \pm 0.5 \times 5.3 \pm 0.4$ | 44° ± 26° | 6.0 ± 0.1 | 45.7 |
| G12.910+0.477 | 18 11 56.751 | −17 30 44.05 | $9.6 \pm 1.1 \times 7.0 \pm 0.9$ | 42° ± 20° | 5.0 ± 0.1 | 45.6 |
| G12.944+0.488 | 18 11 58.314 | −17 28 38.78 | $3.6 \pm 0.6 \times 1.6 \pm 0.7$ | 43° ± 13° | 1.0 ± 0.1 | 45.1 |
| G16.560+0.001 | 18 20 54.977 | −14 31 39.84 | ... | ... | 2.5 ± 0.1 | 45.5 |
| G16.614−0.018 | 18 21 05.386 | −14 29 20.45 | ... | ... | 0.9 ± 0.1 | 45.1 |

Note.—Units of right ascension are hours, minutes, and seconds, and units of declination are degrees, arcminutes, and arcseconds. These parameters were obtained from a map with the primary beam response correction applied.

[a] The flux of Lyman continuum photons $N_{\mathrm{L}}$ was obtained assuming distances of 3.6 and 4.5 kpc.

assuming jet emission. These sources are IRAS 18089−1732(1)b, IRAS 18182−1433a, IRAS 18264−1152b, and IRAS 18308−0841c. They are considered good candidates to be massive young stars with dust emission at 7 mm that could come from a disk or envelope. However, further observations at higher and lower frequencies are required to establish if the detected 7 mm emission is actually coming from dust or from optically thick ionized gas (free-free emission).

4. Two of the sources show spectral indices consistent with ionized outflows: IRAS 18089−1732(1)a and IRAS 18182−1433b. IRAS 18264−1152b shows, in addition to the 7 mm excess, a spectral index consistent with an ionized outflow between 3.6 and 1.3 cm. This last source may then be a combination of thermal jet and disk.

5. Two of the sources show spectral indices consistent with optically thick H ii regions: IRAS 18264−1152a and c.

6. Three of the sources show negative spectral indices that suggest the presence of synchrotron contamination: IRAS 18182−1433c and IRAS 18308−0841a and b. However, these spectral indices could also be due to missing flux density in the higher angular resolution, higher frequency observations. If confirmed with multifrequency matching-beam observations, this synchrotron emission could be an indicator of strong shocks produced by the powerful outflows known to exist in these regions.

7. Finally, we also find that the methanol masers in these regions are systematically associated with radio sources that show slightly rising spectral indices: IRAS 18089−1732(1)a, IRAS 18182−1433b, and IRAS 18264−1152b. This indicates that the methanol maser emission is associated with outflows rather than with disks. The interpretation is that these masers are associated with the presence of compact free-free emission.

Our findings are consistent with the accretion scenario, in which a dynamical collapse of molecular clumps results in the formation of disks and molecular outflows, which then leads to the formation of a massive stellar core. However, in each *IRAS* source we also detected multiple radio sources separated by a few arcseconds, suggesting the formation of groups of massive stars.

L. A. Z. acknowledges the Smithsonian Astrophysical Observatory for a predoctoral fellowship. L. F. R. acknowledges the support of Dirección General de Asuntos del Personal Académico (DGAPA), of Universidad Nacional Autónoma de México (UNAM), and of CONACyT (México). H. B. acknowledges financial support by the Emmy-Noether-Programm of the Deutsche Forschungsgemeinschaft (grant BE2578/1). This research has made use of the SIMBAD database, operated at CDS, Strasbourg, France.

TABLE 6

Flux Densities at 0.7, 1.3, and 3.6 cm of the VLA Continuum Sources

| | | | Flux Density | | | |
|---|---|---|---|---|---|---|
| Source | $\alpha_{2000}$ | $\delta_{2000}$ | 3.6 cm | 1.3 cm | 0.7 cm | Nature |
| 18089−1732(1)a | 18 11 51.451 | −17 31 28.85 | 1.10 ± 0.05 | 1.60 ± 0.04 | 3.00 ± 0.30 | Thermal jet + core |
| 18089−1732(1)b | 18 11 51.571 | −17 31 27.89 | ≤0.20 | ≤0.30 | 2.10 ± 0.30 | H ii region? |
| 18182−1433a | 18 21 09.014 | −14 31 47.62 | ≤0.20 | ≤0.35 | 2.26 ± 0.30 | Core + disk |
| 18182−1433b | 18 21 09.129 | −14 31 48.59 | 0.60 ± 0.05 | 0.80 ± 0.05 | 0.72 ± 0.10 | Thermal jet |
| 18182−1433c | 18 21 09.469 | −14 31 56.93 | 1.65 ± 0.03 | 1.10 ± 0.05 | ≤0.80 | Strong shocks? |
| 18264−1152a | 18 29 14.203 | −11 50 23.80 | ≤0.20 | 0.34 ± 0.10 | 1.30 ± 0.20 | H ii region? |
| 18264−1152b | 18 29 14.356 | −11 50 22.50 | 0.80 ± 0.02 | 1.06 ± 0.07 | 2.70 ± 0.20 | Thermal jet + core |
| 18264−1152c | 18 29 14.406 | −11 50 24.77 | ≤0.20 | 0.44 ± 0.10 | 1.70 ± 0.30 | H ii region? |
| 18308−0841a | 18 33 32.891 | −08 39 18.47 | 11.40 ± 0.05 | 10.30 ± 0.20 | 5.38 ± 0.50 | Strong shocks? |
| 18308−0841b | 18 33 32.904 | −08 39 07.33 | 3.21 ± 0.05 | 2.46 ± 0.10 | ≤0.80 | Strong shocks? |
| 18308−0841c | 18 33 33.120 | −08 39 07.53 | ≤0.60 | ≤0.75 | 2.20 ± 0.40 | Core? |

Note.—Units of right ascension are hours, minutes, and seconds, and units of declination are degrees, arcminutes, and arcseconds.

## REFERENCES

Bally, J., & Zinnecker, H. 2005, AJ, 129, 2281
Beuther, H. 2005, ApJ, 628, 800
Beuther, H., Schilke, P., Menten, K. M., Motte, F., Sridharan, T. K., & Wyrowski, F. 2002a, ApJ, 566, 945
Beuther, H., Schilke, P., Sridharan, T. K., Menten, K. M., Walmsley, C. M., & Wyrowski, F. 2002b, A&A, 383, 892
Beuther, H., Walsh, A., Schilke, P., Sridharan, T. K., Menten, K. M., & Wyrowski, F. 2002c, A&A, 390, 289
Beuther, H., et al. 2002d, A&A, 383, 892
———. 2004a, ApJ, 616, L23
———. 2004b, ApJ, 616, L31
Bonnell, I. A., Bate, M. R., & Zinnecker, H. 1998, MNRAS, 298, 93
Cesaroni, R., Felli, M., Testi, L., Walmsley, C. M., & Olmi, L. 1997, A&A, 325, 725
Cesaroni, R., et al. 1999, A&A, 345, 949
DeBuizer, J. 2003, MNRAS, 341, 277
Garay, G., & Lizano, S. 1999, PASP, 111, 1049
Garay, G., Ramirez, S., Rodríguez, L. F., Curiel, S., & Torrelles, J. M. 1996, ApJ, 459, 193
Gibb, A. G., Hoare, M. G., Wyrowski, F., & Mundy, L. G. 2004, in IAU Symp. 221, Star Formation at High Angular Resolution, ed. M. Burton et al. (San Francisco: ASP), 425
Hildebrand, R. 1983, QJRAS, 24, 267
Jiang, Z. et al. 2005, Nature, 437, 112
Kurtz, S., Hofner, P., & Vargas Alvarez, C. 2004, ApJS, 155, 149
Martí, J., Rodríguez, L. F., & Reipurth, B. 1993, ApJ, 416, 208
McKee, C. F., & Tan, J. C. 2002, Nature, 416, 59
Norberg, P., & Maeder, A. 2000, A&A, 359, 1025
Panagia, N. 1973, AJ, 78, 929
Patel, N., et al. 2005, Nature, 437, 109
Pestalozzi, M. R., Elitzur, M., Conway, J. E., & Booth, R. S. 2004, ApJ, 603, L113
Rodríguez, L. F., Curiel, S., Moran, J. M., Mirabel, I. F., Roth, M., & Garay, G. 1989, ApJ, 346, L85
Rodríguez, L. F., Garay, G., Brooks, K. J., & Mardones, D. 2005, ApJ, 626, 953
Schreyer, K., Henning, Th., Van der Tak, F. F. S., Boonman, A. M. S., van Dishoeck, E. F. 2002, A&A, 394, 561
Shepherd, D. S., Claussen, M. J., & Kurtz, S. E. 2001, Science, 292, 1513
Shepherd, D. S., & Kurtz, S. E. 1999, ApJ, 523, 690
Sridharan, T. K., Beuther, H., Schilke, P., Menten, K. M., & Wyrowski, F. 2002, ApJ, 566, 931
Stahler, S. W., Palla, F., & Ho, P. T. P. 2000, in Protostars and Planets IV, ed. V. Mannings et al. (Tucson: Univ. Arizona Press), 327
Van der Tak, F. F. S., & Menten, K. M. 2005, A&A, 437, 947
Walsh, A. J., Burton, M. G., Hyland, A. R., & Robinson, G. 1998, MNRAS, 301, 640
Wilner, D. J., Reid, M. J., & Menten, K. M. 1999, ApJ, 513, 775
Wolfire, M. G., & Cassinelli, J. P. 1987, ApJ, 319, 850
Yorke, H. W., & Sonnhalter, C. 2002, ApJ, 569, 846
Zhang, Q., Hunter, T. R., & Sridharan, T. K. 1998, ApJ, 505, L151
Zhang, Q., Hunter, T. R., Sridharan, T. K., & Ho, P. T. P. 2002, ApJ, 566, 982